Title

A conserved mechanism for JNK-mediated loss of Notch function in advanced prostate cancer

Journal

Science Signaling, 16(810)

ISSN

1945-0877

Authors

Wang, Cheng-Wei
Clémot, Marie
Hashimoto, Takao
et al.

Publication Date

2023-11-07

DOI

10.1126/scisignal.abo5213

Peer reviewed

Published in final edited form as:

Sci Signal. 2023 November 07; 16(810): eabo5213. doi:10.1126/scisignal.abo5213.

A Conserved Mechanism for JNK-Mediated Loss of Notch Function in Advanced Prostate Cancer

Cheng-Wei Wang[1,#], **Marie Clémot**[1,#,*], **Takao Hashimoto**[1], **Johnny A. Diaz**[1], **Lauren M. Goins**[1], **Andrew S. Goldstein**[1,3,4,5,6], **Raghavendra Nagaraj**[1,*], **Utpal Banerjee**[1,2,4,6,*]

[1]Department of Molecular, Cell and Developmental Biology; University of California, Los Angeles, Los Angeles, CA, USA

[2]Department of Biological Chemistry; University of California, Los Angeles, Los Angeles, CA, USA

[3]Department of Urology, David Geffen School of Medicine, University of California, Los Angeles, Los Angeles, CA, USA

[4]Eli and Edythe Broad Center of Regenerative Medicine and Stem Cell Research, University of California, Los Angeles, Los Angeles, CA, USA

[5]Jonsson Comprehensive Cancer Center, University of California, Los Angeles, Los Angeles, CA, USA

[6]Molecular Biology Institute; University of California, Los Angeles, Los Angeles, CA, USA

Abstract

Dysregulated Notch signaling is a common feature of cancer; however, its effects on tumor initiation and progression are highly variable, with Notch having either oncogenic or tumor-suppressive functions in various cancers. To better understand the mechanisms that regulate Notch function in cancer, we studied Notch signaling in a *Drosophila* tumor model, prostate cancer–derived cell lines, and tissue samples from patients with advanced prostate cancer. We demonstrated that increased activity of the Src-JNK pathway in tumors inactivated Notch signaling due to JNK pathway-mediated inhibition of the expression of the gene encoding the Notch S2 cleavage protease, Kuzbanian, which is critical for Notch activity. Consequently, inactive Notch accumulated in cells, where it was unable to transcribe genes encoding its target proteins, many of which have tumor-suppressive activities. These findings suggest that Src-JNK activity in tumors predicts Notch activity status and that suppressing Src-JNK signaling could restore Notch function

[*]co-corresponding authors (Marie Clémot: mclemot@ucla.edu; Raghavendra Nagaraj: rchavour@ucla.edu; Utpal Banerjee: banerjee@mbi.ucla.edu).

[#]co-first authors

Author Contributions

Conceptualization: CWW, UB; Methodology: CWW, MC, JD,TH; Formal analysis: CWW, MC, LGC, RN, UB; Investigation: CWW, MC, JD, TH, LGC, AG, RN, UB; Funding acquisition: UB; Supervision: AG,RN,UB; Writing: CWW,MC,RN,UB.

Competing Interests

The authors declare that they have no competing interests.

Data Materials Availability

All data needed to evaluate the conclusions are present in the paper or the Supplementary Materials.

in tumors, offering opportunities for diagnosis and targeted therapies for a subset of advanced prostate cancer patients.

Keywords

Notch; JNK; ADAM; Kuzbanian; Prostate Cancer; *Drosophila*

Introduction

First identified and characterized in *Drosophila melanogaster* (1–3), the Notch pathway is a highly evolutionarily conserved signaling mechanism with crucial roles in development and tissue homeostasis (4–7). In order to be activated, the Notch receptor undergoes three proteolytic cleavages at specific sites (schematically depicted in Fig 1A). The first cleavage site, known as S1, is targeted by the protease Furin while the protein transits from the endoplasmic reticulum (ER) to the plasma membrane. Upon interaction of the receptor with a transmembrane ligand on a neighboring cell, Notch is then cleaved at the S2 site by proteases of the ADAM (A disintegrin and metalloprotease) family, principally ADAM10/17 in mammals and Kuzbanian in *Drosophila*. This S2 cleavage leads to the detachment of the Notch extracellular domain (N^{ECD}) and the subsequent intracellular cleavage at the S3 site by the γ-secretase complex. The latter releases the Notch intracellular domain (N^{ICD}), which translocates to the cell nucleus where it interacts with CSL (Suppressor of Hairless in *Drosophila*) to regulate transcription of target genes. Although the resulting signaling outputs are diverse and context-dependent, they converge to control cell fate (6, 7).

Dysregulations of Notch signaling, whether resulting from mutations in Notch itself or through other mechanisms, have been described in a large number of cancers and both hypo- and hyper-activation of the pathway have been associated with tumor formation (6–9). A truncated Notch protein, resulting from a chromosomal translocation and corresponding to N^{ICD}, is detected in increased abundance and contributes to the growth of cancers such as T-cell acute lymphoblastic leukemia (T-ALL), B-cell leukemias, lymphomas of mantle and splenic cells and breast cancer. An alternative scenario in squamous cell carcinomas, gliomas, neuroendocrine tumors, monocytic leukemias and others, indicates that Notch can function as a tumor suppressor. Both scenarios have been explored for prostate cancer with mixed results and possible therapeutic agents that target Notch function have yet to be shown to be fully effective (10, 11). Thus, it appears that Notch function is context-dependent in cancer, as it is in development. However, mechanistic details of a tumor suppressive role remain less explored (12).

In past studies of a glycolytic tumor model in *Drosophila* larvae, we showed that expression of an activated form of the PDGF/VEGF Receptor (Pvr) in the wing imaginal disc is sufficient to cause the formation of large tumors, in which three main signaling pathways, the phosphatidylinositol-3-kinase (PI3K), extracellular signal-regulated kinase (ERK) and c-Jun NH2-terminal kinase (JNK) pathways, are activated (13). Genetic analyses demonstrated that PI3K and ERK signaling together promote the activation of Sima (Hif1 homolog in flies), whereas Src promotes the phosphorylation and subsequent activation of JNK. An

integration of these signals at multiple levels results in production of active JNK and lactate dehydrogenase (LDH), which converge in the establishment and maintenance of the Warburg effect, while decreasing oxidative phosphorylation (see fig. S2A for a redrawing of the schematic in (13)). While PI3K and ERK are major oncogenic pathways (14, 15), the JNK pathway has ambivalent roles in cancer and can be either oncogenic or tumor suppressive (16–18), in a manner similar to that of Notch. In prostate cancer, both of these effects have been proposed for JNK (19). As the Notch pathway is active and plays important roles in wing disc development, the *Drosophila* wing disc tumor model offers an ideal context to investigate the contribution of Notch in tumor progression and its potential relationship with JNK.

In the present study, we combine genetic manipulations in the *Drosophila* wing disc tumor model with observations in prostate cancer-derived cell lines and tissue samples from biopsies of patients with advanced prostate cancer. We show that elevated Src-JNK pathway activity in tumors inactivates Notch signaling, by decreasing the expression of the Notch S2 cleavage protease. Consequently, inactive Notch accumulates in the cell but is unable to transcribe genes encoding its target proteins, many of which share tumor-suppressive activities. Our findings suggest that Src-JNK activity in a tumor is predictive of Notch activity status and suggest that suppressing Src-JNK could restore Notch function in the tumor, offering new perspectives for diagnosis and targeted therapies for advanced prostate cancer.

Results

Changes in Notch 1 cleavage correlate with changes in JNK signaling and LDH-A expression in prostate cancer cell lines

To begin analyzing the role of Notch in prostate cancer, we performed Western blot analyses of prostate-derived cell lines. RWPE-1 are normal prostate immortalized cells, LNCaP are early androgen-sensitive prostate cancer cells and PC3 are advanced androgen independent prostate cancer cells (20).

We used two antibodies that identify the intracellular domain of Notch1. The first (clone D3B8) exclusively detects endogenous levels of Notch1^{ICD} as a 110 kDa fragment resulting from the S3 cleavage of Notch1. The second (clone D1E11) identifies a slightly larger fragment of size 120 kDa that includes both N^{ICD} and the transmembrane domain, which results from the earlier S2 cleavage (Fig. 1A). We found that both antibodies give rise to similar trends. RWPE-1 showed higher amounts of Notch 1 intracellular fragments, while prostate cancer cell lines, in particular PC3, showed significantly lesser amounts of the protein fragments (Fig. 1B–D). We then used a third antibody raised against Notch1^{ECD} that identifies the 180 kDa extracellular fragment resulting from S2 cleavage (Fig. 1A). The readily apparent 180 kDa band seen in RWPE-1 cells was detected in lower amounts in LNCaP cells and was further reduced in PC3 cells (Fig. 1E–F). Together, these data suggested a defect in Notch1 cleavage in prostate cancer cell lines, which should result in loss of Notch function in the tumor-derived cells.

We also analyzed the expression of Notch2, Notch3 and Notch4 in prostate cell lines. Similar to Notch1, we found that Notch3 and Notch4 intracellular fragments resulting from S2 cleavage were significantly less abundant in prostate cancer cell lines (fig. S1A,C–D). Such a decrease was also apparent for Notch2 in LNCaP cells, but not in PC3 cells (fig. S1A–B). While the reason for this difference in Notch 2 is unclear, overall, these results established that cleavage of other Notch isoforms is also altered in prostate cancer cells.

Similar to Notch, the JNK pathway can be oncogenic or tumor suppressive depending on contexts; both effects have been proposed in prostate cancer (18–19, 21–23). In mammals, JNK is encoded by three genes that are alternatively spliced to generate two protein isoforms (46 kDa and 54 kDa) differing in their C-terminal region (24). Western blot analysis of JNK in prostate-derived cell lines indicated that the isoform composition, as well as the total amount of JNK was not identical in RWPE-1, LNCaP and PC3 cells (Fig. 1G). We used an antibody that specifically binds to the phosphorylated, and thus activated, form of JNK (pJNK). We observed that the 46 kDa isoform was the predominant phosphorylated form in these cell lines (Fig. 1G) and that the ratio of the intensities associated with pJNK and total JNK for this 46kDa isoform was significantly higher in PC-3 cells than in RWPE-1 cells and LNCaP cells (Fig. 1H). These results showed that the JNK pathway is activated in advanced prostate cancer cells.

Active JNK contributes to metabolic reprogramming and, as a result, increased lactate dehydrogenase (LDH) expression is seen in *Drosophila* tumors (13). We therefore examined LDH-A expression in prostate cell lines, which is particularly relevant given that inhibition of LDH-A has a protective effect on the progression of prostate cancer (25). Consistent with this notion and with what is known in *Drosophila*, we found that expression of LDH-A was significantly increased in PC3 cells compared to RWPE-1 and LNCaP cells (Fig. 1I–J).

Activated JNK correlates with a loss of Notch activity in *Drosophila* tumors

The observation that changes in Notch 1 cleavage and JNK activity are correlated in prostate cancer cells in vitro prompted us to reexamine the *Drosophila* glycolytic tumor model (13) to investigate potential roles of Notch and mechanisms that link Notch and JNK signaling in these tumors.

Large tumors can be induced by expressing Pvr^{act} along the antero-posterior (A/P) boundary of wing imaginal discs (13). In wild type, this A/P axis is a region defined as the narrow stripe of *dpp*-expressing cells (Fig. 2A). By immunostaining, pJNK was not detected in this region (Fig. 2B). When Pvr^{act} was expressed under the control of a *dpp*-enhancer (*dpp-Gal4>UAS-*Pvr^{act}*,UAS-GFP*), a large tumor formed that consists of *dpp*-expressing cells (Fig. 2C) and shows an increase in pJNK (Fig 2D). These results confirmed our previous observations (13) and further established that the JNK pathway is active in these *Drosophila* tumors. Using antibodies against the *Drosophila* N^{ECD} and N^{ICD}, we detected faint Notch protein expression in wild-type imaginal discs (Fig. 2E–F). As a strong contrast, using either of these antibodies, we detected an accumulation of Notch in the tumor (Fig. 2G–H). Given that increased Notch expression was detected using either antibody, we concluded that full length, uncleaved Notch accumulates in these tumors.

To establish this further, we studied the expression of E(spl) (HES in humans (26)), a direct Notch transcriptional target, which is a reliable marker of Notch pathway activity (27, 28). In wild-type imaginal discs, *E(spl)m8-GFP*, a reporter for *E(spl)* expression (29), was observed along the dorso-ventral (D/V) boundary, indicating the normal site of Notch activation (Fig. 2I–J). Despite the large accumulation of Notch (Fig. 2G–H), expression of *E(spl)* was not detected by GFP fluorescence in tumor cells (Fig. 2K–L). The residual expression of *E(spl)* in the few D/V cells that do not express *dpp*, beyond the margins of the tumor (arrows in Fig. 2K–L), served as an internal control. In addition, the expressions of two other well defined targets of Notch signaling in the wing disc, Cut and Wingless (Wg), were affected in a way similar to that seen for *E(spl)*. Both were expressed at the D/V boundary of the wild-type disc (fig. S2B–C and S2F–G), but neither of these Notch target proteins was expressed in Pvr^{act} tumors (fig. S2D–E and S2H–I). These results established that the accumulated Notch observed in Pvr^{act} tumors is inactive and unable to turn on the expression of downstream target genes. Consistently, RNAi-mediated depletion of Notch in the Pvr^{act} background did not prevent the formation of large tumors (fig. S2J–K and S3L). On the contrary, forced activation of Notch, achieved by overexpressing N^{ICD} (N^{act}) along the A/P boundary, caused the expression of *E(Spl)* to be much enhanced (fig. S2L–O). When N^{act} and Pvr^{act} were co-expressed in the same cells, the tumor recovered the ability to express *E(spl)* and was significantly reduced in size (fig. S2P–S and fig. S3L). Taken together, our data indicated that inactive Notch accumulates in Pvr^{act} tumors and forced activation of Notch decreases tumor size, in agreement with a tumor suppressive role for Notch in this tissue.

JNK controls Notch activity through negative regulation of Kuzbanian

ERK, PI3K and JNK signaling pathways function downstream of Pvr^{act} in the wing disc tumors (13). To investigate whether these pathways contribute to the accumulation of inactive Notch in the tumor, we separately expressed the constitutively active forms, $hRaf^{act}$, $PI3K^{act}$, or $JNKK^{act}$ (hep^{act}) and assessed N^{ICD} accumulation and *E(spl)* expression. $hRaf^{act}$ and $PI3K^{act}$ expression, either individually or in combination, gave rise to tumors, but they did not cause an obvious increase in N^{ICD} staining, nor a suppression of *E(spl)* expression (Fig. 3A–B; fig. S3A–H). In fact, these tumors showed ectopic *E(spl)* reporter expression (fig. S3D,F,H). Activation of the third pathway, JNK, cannot be achieved simply by overexpressing activated *hep* (JNKK), since it is established in *Drosophila* that this genotype causes cell death unless simultaneously protected by active Ras/Raf (17, 30, 31). Active Ras/Raf inhibits the cell death-promoting protein Hid (32, 33), which itself negatively regulates the caspase inhibitor Diap1 (34). Indeed, using cleaved caspase 3 staining, we found that Pvr^{act} tumors did not harbor high cell death, but they did so when combined with Ras^{RNAi} (fig. S3I–J). This increased cleaved caspase 3 staining was suppressed by inactivating JNK (Bsk^{DN}) (fig. S3K). Therefore, we used the genetic combination hep^{act}+*Diap1* and this led to the formation of tumors with an accumulation of N^{ICD} and loss of *E(spl)* expression (Fig. 3C–D). This observation indicated that cells survive in this genetic background and linked inactive Notch accumulation to the JNK pathway. In this system, JNK can be activated by the Src kinase (13). Accordingly, we also found that the triple combination Src^{act}+$PI3K^{act}$+$EGFR^{act}$ (unlike the double combination $PI3K^{act}$+$EGFR^{act}$) phenocopied Pvr^{act} in its accumulation of N^{ICD} and caused a loss of

E(spl) reporter expression in a relatively large tumor (Fig. 3E,F). Thus, the activated JNK pathway was responsible for the accumulation of inactive Notch in the tumor.

As loss of function counterparts to the above observations, a dominant negative form of JNK (bsk^{DN}) or a knockdown of JNKK ($hep^{microRNA}$) in the context of the Pvr^{act} tumor reduced N^{ICD} accumulation and restored *E(spl)* reporter expression, while maintaining a large tumor (Fig. 3G–J and fig. S3L). These data confirmed that JNK is the principal regulator of Notch activity in Prv^{act} tumors.

Results from immunostaining analysis of the whole mount tissue were fully consistent with those from an RNA-Seq analysis of the wing discs with or without tumors (13). The RNA level of *E(spl)* was reduced and that of the JNK pathway transcriptional target, *puckered* (*puc*), was significantly enhanced in Pvr^{act} tumors (Fig. 3K). The RNA-Seq data also revealed that expression of *kuzbanian (kuz)* (35, 36), the closest homolog of ADAM17 (37), which is implicated in the extracellular cleavage of N^{ECD} from the rest of the protein at the S2 site, was also significantly reduced in the tumor background (Fig. 3K). This result was confirmed by a qPCR analysis of the mutant tissue, which showed a significant decrease in *kuz* transcript levels (Fig. 3L). In addition, while a GFP-tagged Kuz protein (38) was undetectable in both wild-type and wing discs expressing Pvr^{act} (Fig. 3M–N), inactivation of JNK in $Pvr^{act}+Bsk^{DN}$ wing disc tumors caused high expression of Kuz-GFP (Fig. 3O), implying that JNK activity negatively regulates Kuz expression.

Next, we observed that *E(spl)* reporter expression was restored when the normal Kuz protein was co-expressed in the Pvr^{act} tumor cells (Fig. 3P–R). Furthermore, co-expression of Bsk^{DN} and Pvr^{act}, which increased Kuz-GFP expression (Fig. 3O), also restored *E(spl)* reporter expression (Fig. 3S). This rescue of *E(spl)* by Bsk^{DN} was blocked if a dominant negative Kuz protein was expressed in the same cells (Fig. 3T), providing further support that JNK inhibition restored *kuz* expression and thereby rescued Notch signaling. Altogether, our data indicated that activation of the JNK pathway downstream of Pvr^{act} is responsible for the accumulation of inactive Notch in the tumor, through negative regulation of the Notch S2 cleavage protease Kuzbanian.

JNK inhibits Kuzbanian expression and Notch activity in *Drosophila* blood cells

Our goal was to determine if human prostate cancer tissue showed similarities to the above model, but first, we asked if our observations could be extended to a second *Drosophila* tissue type of a different origin. The mesoderm-derived *Drosophila* blood cells, in particular the crystal cells (CCs) with platelet/granulocyte-like functions (39), are specified by a Runx protein, Lozenge, only in the presence of an active Notch signal (39). We found that when Pvr^{act} was expressed in these cells using a *lozenge-GAL4* driver, the smooth CC plasma membrane structure exhibited morphological characteristics of invasive macrophages (called plasmatocytes in *Drosophila*), with membrane protrusions that resemble filopodial structures (Fig. 4A–D). We assessed the phosphorylation of JNK by immunostaining in these cells and found that pJNK was significantly increased in Pvr^{act} CCs compared to wild-type (Fig. 4A–D,S), indicating that the pathway was activated upon Pvr^{act} expression in blood cells, as was the case for the imaginal disc tumors.

Known direct Notch transcriptional targets in CCs include Hindsight (Hnt; human RREB1 (40)) and Cut (human Cux (41)). These proteins localized to nuclei in wild-type CCs (Fig. 4E–F and fig. S4A–B), but not in Pvr^{act} CCs (Fig. 4G–H,T and fig. S4C–D). These data are reminiscent of the loss of *E(spl)* reporter, Cut and Wg expression in wing disc tumors and suggest that Notch is also inactivated in Pvr^{act} CCs. To determine if loss of Notch target gene expression in CCs was also dependent on JNK activity, we assessed Hnt and Cut expression in CCs co-expressing Pvr^{act} and hep^{mi}. This resulted in a suppression of ectopic cytoplasmic projections as well as a restoration of Hnt and Cut expression in the nucleus (Fig. 4I–J,T and fig. S4E–F). Therefore, JNK regulates Notch target gene expression in Pvr^{act} CCs. In epithelial tumors, our data indicated that this is through a negative regulation of Kuzbanian expression (Fig. 3K–T). Accordingly, forced expression of Kuz in Pvr^{act} CCs restored the expression of both Notch targets Hnt (Fig. 4K–L,T) and Cut (fig. S4G–L).

kuz-lacZ, a reporter for *kuz* expression, can be used to monitor *kuz* expression levels. We found that compared with the control (Fig. 4 M–N), *kuz* expression was significantly decreased in Pvr^{act} (Fig. 4O–P,U). Co-expression of hep^{mi} with Pvr^{act} increased *kuz-lacZ* expression above that seen in control cells (Fig. 4Q–R,U), indicating that JNK also regulates Kuzbanian expression in CCs. Thus, JNK inhibits Notch pathway activity through the same mechanism in two distinct *Drosophila* cell types upon expression of the Pvr^{act} oncogene.

Low Notch activity correlates with high JNK activity in human prostate cancer tissues

To probe for possible consistency with tumor-derived tissue, we performed immuno-histochemical (IHC) staining on Formalin Fixed Paraffin Embedded (FFPE) sections from human prostate adenocarcinoma tissues obtained from the UCLA prostate cancer repository. Using appropriate antibodies, we found that $Notch1^{ECD}$ was faintly, if at all, detected in benign prostate tissue (Fig. 5A–B). By contrast, we observed an accumulation of $Notch1^{ECD}$ in prostate cancer tissues (Fig. 5C–E). The accumulation inside the cells suggests that this corresponds to uncleaved, and therefore inactive, Notch 1 receptor that saturates the cell surface and is detected in cytoplasmic vesicles (42, 43). Indeed, whereas the Notch1 target protein HES-7 (E(spl)m8 in *Drosophila*) was robustly expressed in the nuclei of benign prostate cells (Fig. 5F–G), its expression was strongly attenuated in the nuclei of prostate cancer cells (Fig. 5H–J). In agreement, an analysis based on the publicly available GEPIA tool (44), for curated RNAseq data obtained from a large collection of prostate adenocarcinomas, indicated that HES-7, in particular, and other Notch targets such as HES-1, HES-5 and HEY-1 to a lesser extent, are negatively regulated in prostate cancer tissue (44). Therefore, as in *Drosophila* wing disc and crystal cells, Notch signaling was found to be active in the normal prostate tissue, but became inhibited as Notch accumulated in an inactive form in advanced prostate cancer. We also observed an increase in pJNK-associated staining in advanced prostate cancer tissue when compared with benign tissue (Fig. 5K–O). Thus, the JNK pathway is active in tumors of patients with advanced prostate cancer but not in the benign tissue. Finally, qualitative analysis of LDH-A staining in benign prostate tissue and advanced prostate cancer biopsy samples suggested that these tumors are glycolytic (fig. S5). These observations correlated with those seen in *Drosophila*, leading to the conclusion that activation of JNK in advanced prostate cancer leads to inactivation of the Notch pathway through similar mechanisms in an evolutionarily conserved manner.

Discussion

Notch and JNK are two signaling pathways that play important roles in cancer and both have been alternately described as oncogenic or tumor suppressive in a context-dependent manner (8, 9, 18). As therapeutic strategies aimed at modulating the activity of these pathways are being developed (19, 45), it is crucial to be able to predict how they function in a particular tumor, in order to help make better informed treatment decisions.

In the present study, we took advantage of a well characterized *Drosophila* tumor model to uncover a mechanism by which activation of the JNK pathway can lead to inhibition of Notch signaling. In the imaginal wing disc epithelium, expression of a single oncogene, Pvr^{act}, causes the formation of large tumors in which the JNK pathway is activated. We demonstrated that, although the Notch protein accumulates in these tumors, it is largely inactive, as indicated by the lack of expression of Notch target genes. Using a genetic approach, we showed that decreasing JNK activity was sufficient to restore Notch activity in the tumor. We found that in this system, JNK inhibits the expression of the Notch S2 cleavage protease Kuzbanian, thereby preventing Notch activation. We showed that the same occurs in a population of *Drosophila* blood cells expressing the Pvr^{act} oncogene.

In parallel, we found a similar correlation between activation of JNK and accumulation of inactive Notch in prostate cancer cell lines and in prostate tissue samples derived from patients with advanced prostate cancer, suggesting that this mechanism is conserved through evolution. Accordingly, we found by Western-blot analysis that PC3 cells, derived from advanced prostate cancer, exhibit a defect in Notch cleavage at the S2 site and work by others has shown that, at a transcript level, PC3 cells express decreased amounts of the S2 protease ADAM17 (46).

The functional observations in the two different tissue types in *Drosophila* and the expression patterns in human prostate cancer cell lines and primary tumor samples, when taken together, support the model shown in Figure 6 (Fig. 6A–B). The model suggests that if cells with developmentally active Notch signaling, such as the luminal cells of the normal prostate, acquire an activating mutation in JNK or an upstream kinase such as Src, this would cause loss of a Notch S2 cleavage enzyme and result in accumulation of inactive, full-length Notch, which is unable to support the expression of its downstream targets. This model provides one mechanism through which Notch can act as a tumor suppressor. Many Notch target proteins are necessary to maintain tissue integrity and epithelial morphology (47). For example, some target proteins, such as HES and RREB, are essential in maintaining normal growth, whereas others, such as Cux, enable differentiation (40, 41). The combined results from this comparative analysis, in which functional relevance is established using genetic dissection in *Drosophila* and correlation to a human cancer, illustrates how context dependence can determine alternative ways to achieve an oncogenic *vs* a tumor suppressive mode (48–51). The most parsimonious interpretation of the model is that Notch can have a tumor suppressive role in prostate cancers that have activated JNK. These findings suggest that Src-JNK activation in a tumor can be predictive of the activity status of Notch.

Therefore, therapeutic strategies for advanced prostate cancer might benefit from identifying molecules that block JNK or its upstream components and those that facilitate controlled activation of Notch, rather than drugs that inhibit Notch function, as these are expected to work only for contexts where Notch functions as an oncogene. On the other hand, JNK activation could simultaneously have additional tumor suppressive effects, for example by inducing apoptosis, and therefore inhibiting all JNK activity may not always be beneficial for treatment. Further investigation is needed to elucidate the mechanism by which JNK regulates Notch1 proteolytic cleavage and activity in prostate cancer, as this could contribute to the refinement of drug design strategies to target downstream effectors and potentially maintain normal JNK functions.

Materials and Methods

Cell lines

Cell lines used in this study were acquired from the American Type Culture Collection (ATCC) and are the following: RWPE-1 (non-transformed human prostate epithelial cell line, ATCC CRL-11609), LNCaP (androgen receptor-positive prostate cancer cell line, ATCC CRL-1740), PC3 (androgen receptor-negative prostate cancer cell line, ATCC CRL-1435). Cells were cultured according to ATCC's protocols. The cell identities were validated by a short tandem repeat-based authentication service (Laragen).

Immunoblotting of prostate cancer cell line samples

Protein lysates from prostate cancer cell lines were prepared by lysing the cells with RIPA buffer (Thermo Scientific ref. 89901) supplemented with protease inhibitors (cOmplete Protease Inhibitor Cocktail, Roche ref. 11836153001) and phosphatase inhibitors (Halt Phosphatase Inhibitor Cocktail, Thermo Scientific ref. 78428). For Western blotting, 20 μg of protein were loaded into each lane. Antibodies and their dilutions used are as follows: rabbit anti-Notch1^{ECD} (1:1000; Millipore Sigma #07–218), mouse anti-pJNK (1:500; G-7, Santa Cruz Biotechnology #sc-6254), rabbit anti-JNK (1:500, Cell Signaling Technology #9252) mouse anti-LDH-A (1:2000; 5D2.1, Millipore MABC150), rabbit anti-cleaved Notch1 (Val1744) (1:1000; D3B8, Cell Signaling Technology #4147), rabbit anti-Notch1 (1:1000; D1E11, Cell Signaling Technology #3608), rabbit anti-Notch2 (1:1000; Cell Signaling Technology #5732), rabbit anti-Notch3 (1:1000; Cell Signaling Technology #5276), mouse anti-Notch4 (1:1000; Cell Signaling Technology #2423), mouse anti-alpha-tubulin (1:100; Developmental Study Hybridoma Bank 12G10), mouse anti-GAPDH (1:2000; Proteintech #60004–1-Ig), HRP-conjugated goat anti-rabbit IgG (1:10000; Invitrogen #31463) and HRP-conjugated goat anti-mouse IgG (1:10000; Invitrogen #31430). Chemiluminescent signals were obtained using ECL Prime Western Blotting Detection Reagent (Amersham ref. RPN2236) and iBright FL1500 Imaging System (Invitrogen ref. A44115), and with SuperSignal West Pico PLUS (Thermo Scientific ref. 34577) and West Atto (Thermo Scientific ref. 38554) substrates. Total protein was visualized by No-Stain Protein Labeling Reagent (Invitrogen ref. A44717). Quantification of the Western blots was performed using the ImageJ image analysis software.

Fly stocks and genetics

The *Drosophila* stocks used in this study are the following: w^{1118}, *dpp-GAL4*$^{blk-1}$ (BDSC#93385), *lozenge-GAL4* (BDSC#6314) *UAS-Pvr*^{act} (λ-Pvr) (Norbert Perrimon), *E(spl)m8-GFP* (James W. Posakony), *UAS-cRaf1*^{gof} (*hRaf*^{act}, BDSC#2074), *UAS-dp110*^{CAAX} (*PI3K*^{act}, BDSC#25908), *UAS-hep*^{act} (BDSC#9306), *UAS-dIAP1* (BDSC#6657), *UAS-src42*^{act} (BDSC#6410), *UAS-Bsk*^{DN} (BDSC #9311), *UAS-hep*^{microRNA} (*hep*^{mi}, Guang-Chao Chen), *kuz-GFP* (François Schweisguth), *UAS-kuz* (BDSC#5816), *UAS-kuz*^{DN} (BDSC#6578), *kuz-lacZ* (BDSC#10505), *UAS-N*^{act} (Yuh-Nung Jan), *UAS-EGFR*^{act} (Trudi Schupbach). All fly stocks were raised on standard cornmeal medium at 25°C. Cell-type specific induction of transgene expression was performed using the binary *GAL4/UAS* system (52).

Immunostaining of *Drosophila* tissues

For immunofluorescent staining of *Drosophila* imaginal wing discs, wandering 3rd instar larvae were dissected in PBS, fixed for 30min in 4% paraformaldehyde, washed and permeabilized in 0.3% PBT (1x PBS, 0.1% Triton X-100). Tissues were incubated in 3% Bovine Serum Albumin (BSA)-0.1% PBT blocking solution for at least 30 minutes. Following overnight incubation with primary antibodies at 4°C, samples were washed with PBT three times for 15 minutes, incubated with secondary antibodies (Invitrogen, 1:500 in blocking solution) for 2h at room temperature, washed with PBT three times for 15 minutes and mounted in Vectashield® with DAPI (H-1200, Vector laboratories).

For staining of circulating hemocytes, wandering 3rd instar larvae were bled in PBS on 8-well glass slide in a humid chamber (one larva per well). Hemocytes were allowed to settle for 30min, before replacing the PBS with a drop of fixative solution (6% paraformaldehyde in PBS). After 30min fixation, hemocytes were washed and permeabilized in 0.3% PBT, incubated with blocking solution (3% BSA in PBT) for at least 30min and with primary antibodies overnight at 4°C. After washes in 0.3% PBT, hemocytes were incubated with secondary antibodies for 2h at room temperature, washed in PBT, stained with DAPI (1:1000 in PBS) for 10min and washed in PBS. Finally, PBS was replaced by a drop of Vectashield Vibrance® hardening antifade mounting medium (H-1700).

Primary antibodies were diluted in blocking solution as follow: mouse anti-NotchECD (1:50; C458.2H, DSHB), mouse anti-NotchICD (1:50; C17.9C6, DSHB), rabbit anti-pJNK (Thr183/Tyr185) (1:500; Cell Signaling #9251), mouse anti-Hnt (1:200; 1G9, DSHB), mouse anti-Cut (1:100; 2B10, DSHB) and mouse anti-Wg (1:5; 4D4, DSHB). Alexa-conjugated secondary antibodies (Invitrogen) were diluted 1:500 in blocking solution.

Quantitative Real-Time PCR Analysis

Total RNA was extracted from ~40 3rd instar imaginal wing discs using PureLink RNA mini kit (Ambion). The SuperScript III First-Strand synthesis SuperMix kit (Invitrogen) was used for first-strand cDNA synthesis. Relative quantitative PCR was performed by comparative CT method using Power SYBR Green PCR master mix kit (Applied Biosystems) and a StepOne Real-Time PCR detection thermal cycler (Applied Biosystems) using RT2 qPCR

Primer Assay (SA Biosciences, QIAGEN), with primers specific for genes of interest and *RpL10* (PPD10569B). The levels of *RpL10* were used to normalize total cDNA input.

Prostate tissue samples

Formalin Fixed Paraffin-embedded tissue sections from localized prostate adenocarcinoma and adjacent benign prostate tissue were provided by the Translational Pathology Core Laboratory (TPCL) at UCLA. All samples were collected from patients with informed consent, and all related procedures were performed with the approval of the internal review and ethics boards.

Immunohistochemistry

For immunohistochemistry on human prostate tissue samples, paraffin-embedded tissue sections were incubated in a 60°C oven for 1hr and de-paraffinized in three changes of xylene, followed by 100% alcohol twice for 3 min each. Then the slides were transferred once in 95% and 70% alcohol, each for 3 min. A heat antigen retrieval step was used to unmask the antigenic epitopes. The remaining procedure was performed using HRP-DAB Cell and Tissue Staining Kits (CTS002 and CTS005, R&D Systems) according to the manufacturer's protocol. Primary antibodies used for staining are: rabbit anti-NotchECD (1:500; Millipore Sigma #07–218), rabbit anti-pJNK (Thr183/Tyr185) (1:500; Cell Signaling #9251), rabbit anti-HES7 (1:100; Invitrogen #PA5–73023) and mouse anti-LDH-A (1:1000; 5D2.1, Millipore MABC150). Biotinylated anti-mouse (CTS002, R&D Systems) and anti-rabbit (CTS005, R&D Systems) secondary antibodies are parts of the HRP-DAB Cell and Tissue staining kits.

Microscopy and image analysis

Fluorescent images were acquired with a Zeiss LSM 880 confocal microscope and ZEN 2018 acquisition software. Images were analyzed with the ImageJ software. All images shown are representative images of at least three independent experiments. Images of immunohistochemistry experiments were acquired with a fluorescence compound microscope with bright field imaging capability.

To quantify the ratio of the *dpp* positive area over the whole disc area in *Drosophila* imaginal discs, a reporter for *dpp* expression (*UAS-GFP* or *UAS-mCherry*) was used to delimitate the area of the *dpp* positive area, and nuclear staining with DAPI was used to delimitate the disc area. Statistical significance was evaluated using the software Graphpad Prism v6.0, after verifying the normality of values and equivalence of variances. Graphics display means with standard deviations and the statistical differences between control and test samples were assessed using unpaired t-tests.

To measure the staining intensity in IHC images, the Colour deconvolution function in the Fiji image analysis software was used. This function was created based on the method by Ruifrok and Johnston (53) to determine the relative contribution of each of the RGB color channels to the DAB staining. For N^{ECD}, pJNK and LDH-A stainings, the mean intensity in the deconvolved DAB images was measured in 40 to 60 square regions of identical size spanning the tissue sections in areas containing cells (avoiding regions devoid of tissue).

For HES7, nuclei were segmented using hematoxylin staining and the mean intensity per nucleus was measured on the deconvolved DAB images. The integrated optical density (OD), referred to as “relative intensity”, was calculated as OD=log (maximum intensity/measured intensity), where the maximum intensity was determined for each image as the average mean intensity in lumen areas (devoid of cells). For each staining, three benign prostate tissue sample and three advanced prostate tumor samples (from different patients) were analyzed and the average relative intensity per sample was calculated. For each tumor sample, the relative intensity fold change compared to the average of the relative intensity of the three benign tissue samples, was calculated and plotted in Figure 5. In instances where the tissue sample contained both normal tubular tissue and prostate cancer tissue with disrupted tubules, the quantitative measures were applied to the morphologically affected parts.

Supplementary Material

Refer to Web version on PubMed Central for supplementary material.

Acknowledgments

We thank members of the Banerjee laboratory for support, intellectual input, and technical expertise. We thank UCLA’s Translational Pathology Core Laboratory. We thank Arunima Purkayastha (University of California, Los Angeles) for generating RNA seq data. We thank James Posakony (University of California, San Diego), Norbert Perrimon (Harvard University), Guang-Chao Chen (Institute of Biological Chemistry, Academia Sinica), François Schweisguth (Institut Pasteur), Yuh-Nung Jan (University of California, San Francisco) and Trudi Schüpbach (Princeton University) for kindly providing fly stocks, as well as the Vienna (VDRC) and Bloomington (BDSC) *Drosophila* stock centers.

Funding

MC was supported by a UCLA Broad Stem Cell Research Center training grant. LMG was supported by a Ruth L Kirschstein Institutional NRSA T32CA009056 and by NHLBI 3R01HL067395–16S1. We are grateful for the support provided to UB for most of this work by NIH R01 CA-217608 and partly by NIH R01 HL-067395.

References

1. Kidd S, Lockett TJ, Young MW, The Notch locus of Drosophila melanogaster. Cell. 34, 421–433 (1983). [PubMed: 6193889]
2. Knust E, Campos-Ortega JA, The molecular genetics of early neurogenesis in Drosophila melanogaster. BioEssays. 11 (1989), pp. 95–100. [PubMed: 2515857]
3. Wharton KA, Johansen KM, Xu T, Artavanis-Tsakonas S, Nucleotide sequence from the neurogenic locus Notch implies a gene product that shares homology with proteins containing EGF-like repeats. Cell. 43, 567–581 (1985). [PubMed: 3935325]
4. Artavanis-Tsakonas S, Rand MD, Lake RJ, Notch signaling: Cell fate control and signal integration in development. Science (80-.). 284 (1999), pp. 770–776.
5. Bray S, Notch signalling: a simple pathway becomes complex. Nat. Rev. Mol. Cell Biol. 7, 678–689 (2006). [PubMed: 16921404]
6. Siebel C, Lendahl U, Notch signaling in development, tissue homeostasis, and disease. Physiol. Rev. 97, 1235–1294 (2017). [PubMed: 28794168]
7. Zhou B, Lin W, Long Y, Yang Y, Zhang H, Wu K, Chu Q, Notch signaling pathway: architecture, disease, and therapeutics. Signal Transduct. Target. Ther. 7, 1–33 (2022). [PubMed: 34980881]
8. Radtke F, Raj K, The role of Notch in tumorigenesis: Oncogene or tumour suppressor. Nat. Rev. Cancer. 3, 756–767 (2003). [PubMed: 14570040]

9. Aster JC, Pear WS, Blacklow SC, The Varied Roles of Notch in Cancer. Annu. Rev. Pathol. Mech. Dis. 12 (2017), pp. 245–275.
10. Deng G, Ma L, Meng Q, Ju X, Jiang K, Jiang P, Yu Z, Notch signaling in the prostate: critical roles during development and in the hallmarks of prostate cancer biology. J. Cancer Res. Clin. Oncol. 142 (2016), pp. 531–547. [PubMed: 25736982]
11. Carvalho FLF, Simons BW, Eberhart CG, Berman DM, Notch signaling in prostate cancer: A moving target. Prostate. 74, 933–945 (2014). [PubMed: 24737393]
12. Nowell CS, Radtke F, Notch as a tumour suppressor. Nat. Rev. Cancer. 17 (2017), pp. 145–159. [PubMed: 28154375]
13. Wang CW, Purkayastha A, Jones KT, Thaker SK, Banerjee U, In vivo genetic dissection of tumor growth and the Warburg effect. Elife. 5 (2016), doi:10.7554/eLife.18126.
14. Hoxhaj G, Manning BD, The PI3K-AKT network at the interface of oncogenic signalling and cancer metabolism. Nat. Rev. Cancer. 20, 74–88 (2020). [PubMed: 31686003]
15. Moore AR, Rosenberg SC, McCormick F, Malek S, RAS-targeted therapies: is the undruggable drugged? Nat. Rev. Drug Discov. 19, 533–552 (2020). [PubMed: 32528145]
16. Wagner EF, Nebreda ÁR, Signal integration by JNK and p38 MAPK pathways in cancer development. Nat. Rev. Cancer. 9 (2009), pp. 537–549. [PubMed: 19629069]
17. La Marca JE, Richardson HE, Two-Faced: Roles of JNK Signalling During Tumourigenesis in the Drosophila Model. Front. Cell Dev. Biol. 8 (2020), p. 42. [PubMed: 32117973]
18. Tournier C, The 2 Faces of JNK Signaling in Cancer. Genes and Cancer. 4 (2013), pp. 397–400. [PubMed: 24349637]
19. Xu R, Hu J, The role of JNK in prostate cancer progression and therapeutic strategies. Biomed. Pharmacother. 121 (2020), p. 109679.
20. Sobel RE, Sadar MD, Cell lines used in prostate cancer research: A compendium of old and new lines - Part 1. J. Urol. 173 (2005), pp. 342–359. [PubMed: 15643172]
21. Yang YM, Bost F, Charbono W, Dean N, McKay R, Rhim JS, Depatie C, Mercola D, C-Jun NH2-terminal kinase mediates proliferation and tumor growth of human prostate carcinoma. Clin. Cancer Res. 9, 391–401 (2003). [PubMed: 12538493]
22. Hübner A, Mulholland DJ, Standen CL, Karasarides M, Cavanagh-Kyros J, Barrett T, Chi H, Greiner DL, Tournier C, Sawyers CL, Flavell RA, Wu H, Davis RJ, JNK and PTEN cooperatively control the development of invasive adenocarcinoma of the prostate. Proc. Natl. Acad. Sci. U. S. A. 109, 12046–12051 (2012). [PubMed: 22753496]
23. Parra E, Ferreira J, Modulation of the response of prostate cancer cell lines to cisplatin treatment using small interfering RNA. Oncol. Rep. 30, 1936–1942 (2013). [PubMed: 23900581]
24. Davis RJ, Signal transduction by the JNK group of MAP kinases. Cell. 103 (2000), pp. 239–252. [PubMed: 11057897]
25. Xian ZY, Liu JM, Chen QK, Chen HZ, Ye CJ, Xue J, Yang HQ, Li JL, Liu XF, Kuang SJ, Inhibition of LDHA suppresses tumor progression in prostate cancer. Tumor Biol. 36, 8093–8100 (2015).
26. Bessho Y, Miyoshi G, Sakata R, Kageyama R, Hes7: A bHLH-type repressor gene regulated by Notch and expressed in the presomitic mesoderm. Genes to Cells. 6, 175–185 (2001). [PubMed: 11260262]
27. Ligoxygakis P, Bray SJ, Apidianakis Y, Delidakis C, Ectopic expression of individual E(spl) genes has differential effects on different cell fate decisions and underscores the biphasic requirement for Notch activity in wing margin establishment in Drosophila. Development. 126, 2205–2214 (1999). [PubMed: 10207145]
28. De Celis JF, Tyler DM, De Celis J, Bray SJ, Notch signalling mediates segmentation of the Drosophila leg. Development. 125, 4617–4626 (1998). [PubMed: 9806911]
29. Trylinski M, Mazouni K, Schweisguth F, Intra-lineage Fate Decisions Involve Activation of Notch Receptors Basal to the Midbody in Drosophila Sensory Organ Precursor Cells. Curr. Biol. 27, 2239–2247.e3 (2017). [PubMed: 28736165]
30. Morata G, Shlevkov E, Pérez-Garijo A, Mitogenic signaling from apoptotic cells in Drosophila. Dev. Growth Differ. 53, 168–176 (2011). [PubMed: 21338343]

31. Shlevkov E, Morata G, A dp53/JNK-dependant feedback amplification loop is essential for the apoptotic response to stress in Drosophila. Cell Death Differ. 19, 451–460 (2012). [PubMed: 21886179]
32. Bergmann A, Agapite J, McCall K, Steller H, The Drosophila gene hid is a direct molecular target of ras-dependent survival signaling. Cell. 95, 331–341 (1998). [PubMed: 9814704]
33. Kurada P, White K, Ras promotes cell survival in Drosophila by downregulating hid expression. Cell. 95, 319–329 (1998). [PubMed: 9814703]
34. Wang SL, Hawkins CJ, Yoo SJ, Müller HAJ, Hay BA, The Drosophila caspase inhibitor DIAP1 is essential for cell survival and is negatively regulated by HID. Cell. 98, 453–463 (1999). [PubMed: 10481910]
35. Pan D, Rubin GM, Kuzbanian controls proteolytic processing of Notch and mediates lateral inhibition during Drosophila and vertebrate neurogenesis. Cell. 90, 271–280 (1997). [PubMed: 9244301]
36. Lieber T, Kidd S, Young MW, Kuzbanian-mediated cleavage of Drosophila Notch. Genes Dev. 16, 209–221 (2002). [PubMed: 11799064]
37. Bozkulak EC, Weinmaster G, Selective Use of ADAM10 and ADAM17 in Activation of Notch1 Signaling. Mol. Cell. Biol. 29, 5679–5695 (2009). [PubMed: 19704010]
38. Dornier E, Coumailleau F, Ottavi JF, Moretti J, Boucheix C, Mauduit P, Schweisguth F, Rubinstein E, Tspanc8 tetraspanins regulate ADAM10/Kuzbanian trafficking and promote Notch activation in flies and mammals. J. Cell Biol. 199, 481–496 (2012). [PubMed: 23091066]
39. Banerjee U, Girard JR, Goins LM, Spratford CM, Drosophila as a genetic model for hematopoiesis. Genetics. 211, 367–417 (2019). [PubMed: 30733377]
40. Baechler BL, McKnight C, Pruchnicki PC, Biro NA, Reed BH, Hindsight/RREB-1 functions in both the specification and differentiation of stem cells in the adult midgut of Drosophila. Biol. Open. 5, 1–10 (2016).
41. Cubelos B, Sebastián-Serrano A, Kim S, Redondo JM, Walsh C, Nieto M, Cux-1 and Cux-2 control the development of Reelin expressing cortical interneurons. Dev. Neurobiol. 68, 917–925 (2008). [PubMed: 18327765]
42. Fortini ME, Bilder D, Endocytic regulation of Notch signaling. Curr. Opin. Genet. Dev. 19, 323–328 (2009). [PubMed: 19447603]
43. Steinbuck MP, Winandy S, A review of Notch processing with new insights into ligand-independent notch signaling in T-cells. Front. Immunol. 9, 1230 (2018). [PubMed: 29910816]
44. Tang Z, Li C, Kang B, Gao G, Li C, Zhang Z, GEPIA: A web server for cancer and normal gene expression profiling and interactive analyses. Nucleic Acids Res. 45, W98–W102 (2017). [PubMed: 28407145]
45. Allen F, Maillard I, Therapeutic Targeting of Notch Signaling: From Cancer to Inflammatory Disorders. Front. Cell Dev. Biol. 9, 1–17 (2021).
46. McCulloch DR, Harvey M, Herington AC, The expression of the ADAMs proteases in prostate cancer cell lines and their regulation by dihydrotestosterone. Mol. Cell. Endocrinol. 167, 11–21 (2000). [PubMed: 11000516]
47. Wang Z, Li Y, Kong D, Sarkar FH, The Role of Notch Signaling Pathway in Epithelial-Mesenchymal Transition (EMT) During Development and Tumor Aggressiveness. Curr. Drug Targets. 11, 745–751 (2010). [PubMed: 20041844]
48. Lobry C, Oh P, Mansour MR, Thomas Look A, Aifantis I, Notch signaling: Switching an oncogene to a tumor suppressor. Blood. 123 (2014), pp. 2451–2459. [PubMed: 24608975]
49. Lobry C, Oh P, Aifantis I, Oncogenic and tumor suppressor functions of Notch in cancer: It's NOTCH what you think. J. Exp. Med. 208 (2011), pp. 1931–1935. [PubMed: 21948802]
50. Zhang L, Sha J, Yang G, Huang X, Bo J, Huang Y, Activation of Notch pathway is linked with epithelial-mesenchymal transition in prostate cancer cells. Cell Cycle. 16, 999–1007 (2017). [PubMed: 28388267]
51. Marignol L, Rivera-Figueroa K, Lynch T, Hollywood D, Hypoxia, notch signalling, and prostate cancer. Nat. Rev. Urol. 10 (2013), pp. 405–413. [PubMed: 23712204]
52. Brand AH, Perrimon N, Targeted gene expression as a means of altering cell fates and generating dominant phenotypes. Development. 118, 401–15 (1993). [PubMed: 8223268]

53. Ruifrok AC, Johnston DA, Quantification of histochemical staining by color deconvolution. Anal. Quant. Cytol. Histol. 23, 291–299 (2001). [PubMed: 11531144]

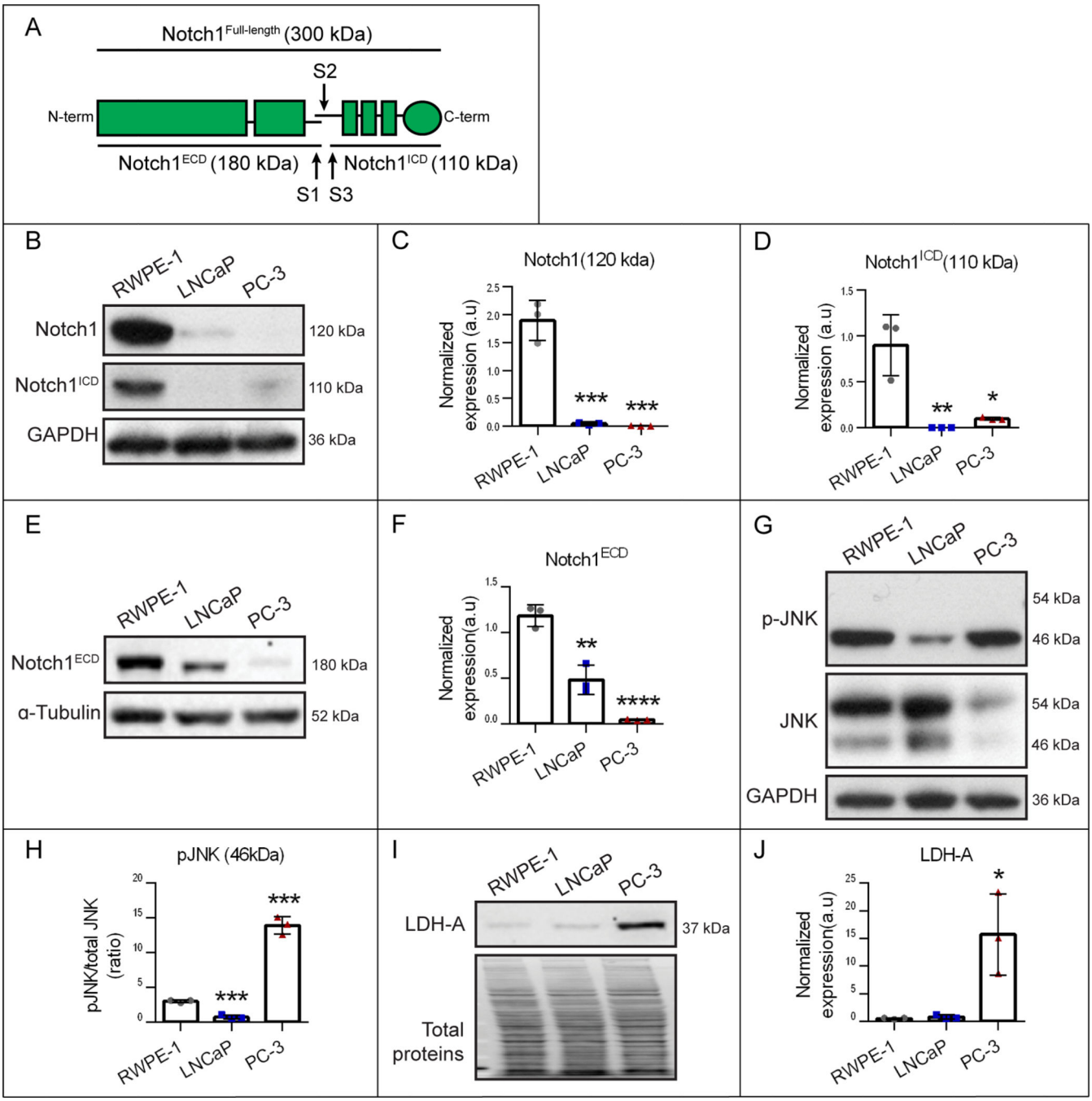

Fig. 1. Change in Notch 1 cleavage correlates with changes in JNK signaling and LDH-A expression in prostate cancer cell lines.

(A) Schematic of the Notch 1 receptor depicting the 3 cleavage sites: S1, S2, and S3, with the resulting extracellular domain (ECD) and intracellular domain (ICD) fragments.

(B-J) Immunoblots of cell extracts from benign prostate (RWPE-1), early stage prostate cancer (LNCaP) and androgen resistant prostate cancer (PC-3) cell lines.

(B-D) Immunodetection of Notch 1 (N^{ICD} plus transmembrane fragment, 120 kDa), $Notch1^{ICD}$ (110 kDa) and GAPDH (36 kDa) as a loading control **(B)**. Quantification of

the normalized expression of the 120 kDa Notch1 fragment **(C)** and the 110 kDa Notch1^{ICD} **(D)** in each cell line is shown as the ratio of the corresponding signal intensity over the corresponding GAPDH-associated signal intensity.

(E-F) Immunodetection of Notch 1 extracellular domain (Notch1^{ECD}, 180 kDa) and α-tubulin (52 kDa) as a loading control **(E)**. Quantification of the normalized expression of Notch1^{ECD} in each cell line is shown as the ratio of the 180 kDa Notch1^{ECD}-associated signal intensity scaled against the corresponding GAPDH-associated signal intensity **(F)**.

(G-H) Immunodetection of phosphorylated JNK (pJNK, 46kDa), total JNK (46 kDa, 54 kDa) and GAPDH (36 kDa) as a loading control **(G)**. Quantification of the relative levels of pJNK in each cell line is shown as the ratio of the 46kDa pJNK and the corresponding 46kDa total JNK band **(H)**.

(I-J) Immunodetection of LDH-A (37 kDa) and total protein staining **(I)**. Quantification of the normalized levels of LDH-A in each cell line is shown as the ratio of LDH-A-associated signal intensity over total protein staining intensity **(J)**.

Unpaired t-tests were used to evaluate statistical significance, denoted as * for $0.01<p\leq 0.05$, ** for $0.05<p\leq 0.01$ and *** for $0.01<p\leq 0.001$. Comparisons were performed between RWPE-1 and LNCaP cells and between RWPE-1 and PC-3 cells. For quantification of each immunoblot, N=3 biological replicates were used that were derived from independent cell lysates.

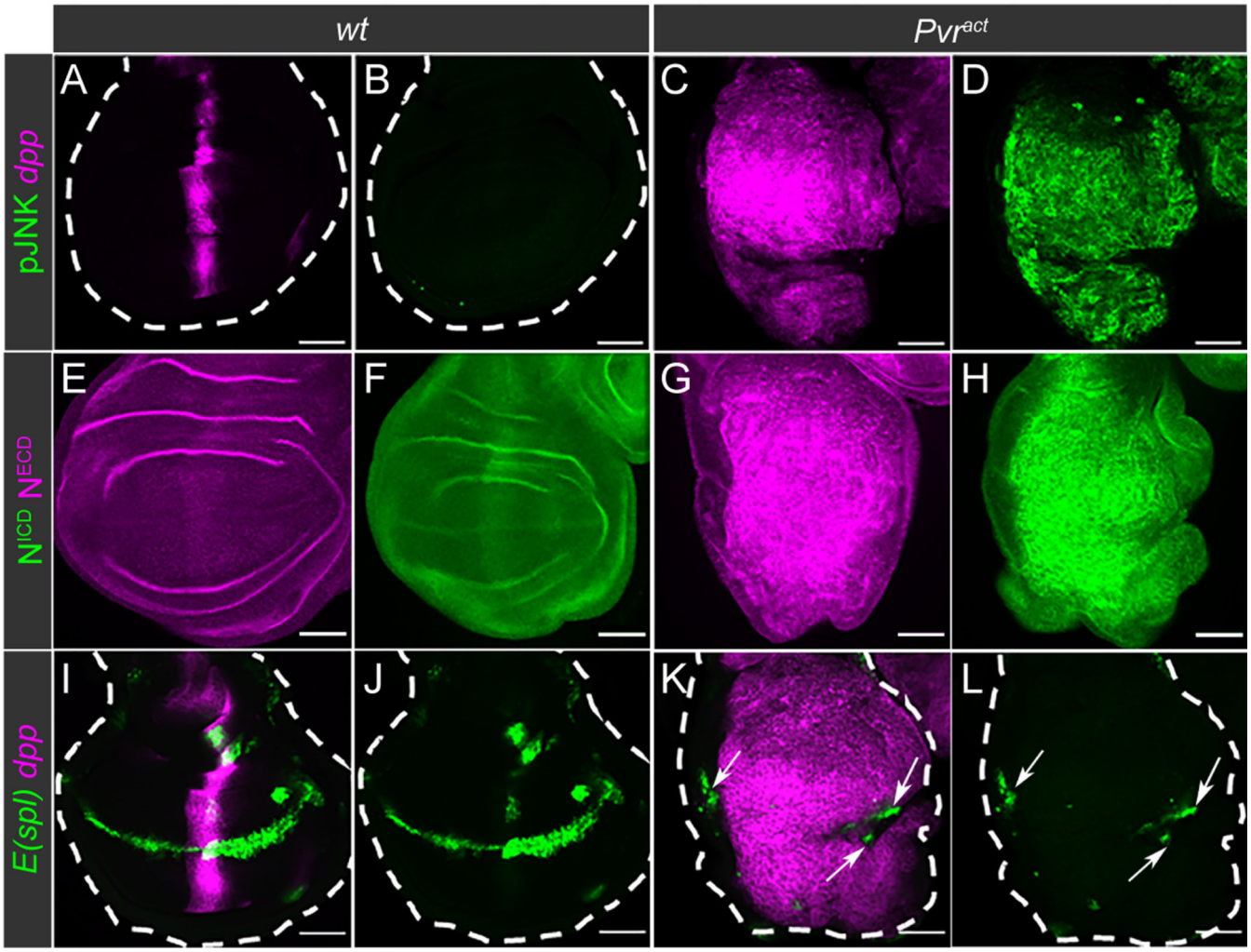

Fig. 2. Activation of JNK correlates with loss of Notch activity in *Drosophila* tumors

(A-L) Immunostaining of *Drosophila* wing imaginal discs from wandering third instar larvae, with wild-type (*wt*) as control compared with Pvr^{act}. *wt* larvae express mCherry alone (magenta; *dpp-GAL4>UAS-mCherry::CD8*) and Pvr^{act} larvae express mCherry and Pvr^{act} (*dpp-GAL4>UAS-mCherry::CD8,UAS-*Pvr^{act}) along the A/P boundary of the wing discs.

(A-D) Activity of the JNK pathway, assessed by immunostaining of pJNK (green; **B, D**), in *wt* (**A-B**) and Pvr^{act} (**C-D**) wing discs. The *dpp*-expressing cells are identified by mCherry expression (magenta; **A, C**).

(E-H) Immunostaining of Notch with anti-N^{ECD} (magenta; **E,G**) and anti-N^{ICD} (green; **F,H**) antibodies, in *wt* (**E-F**) and Pvr^{act} (**G-H**) wing discs.

(I-L) Expression of the *E(spl)m8-GFP* reporter (green) in *wt* (**I-J**) and Pvr^{act} (**K-L**) wing discs. The *dpp*-expressing cells are identified by mCherry expression (magenta; **I,K**). Arrows in K-L point to *E(spl)m8-GFP* expression outside of the *dpp*-expressing region. Each staining was repeated 3 times (N=3) and between 5 and 15 samples were analyzed per repeat.

Scale bars: 50μm.

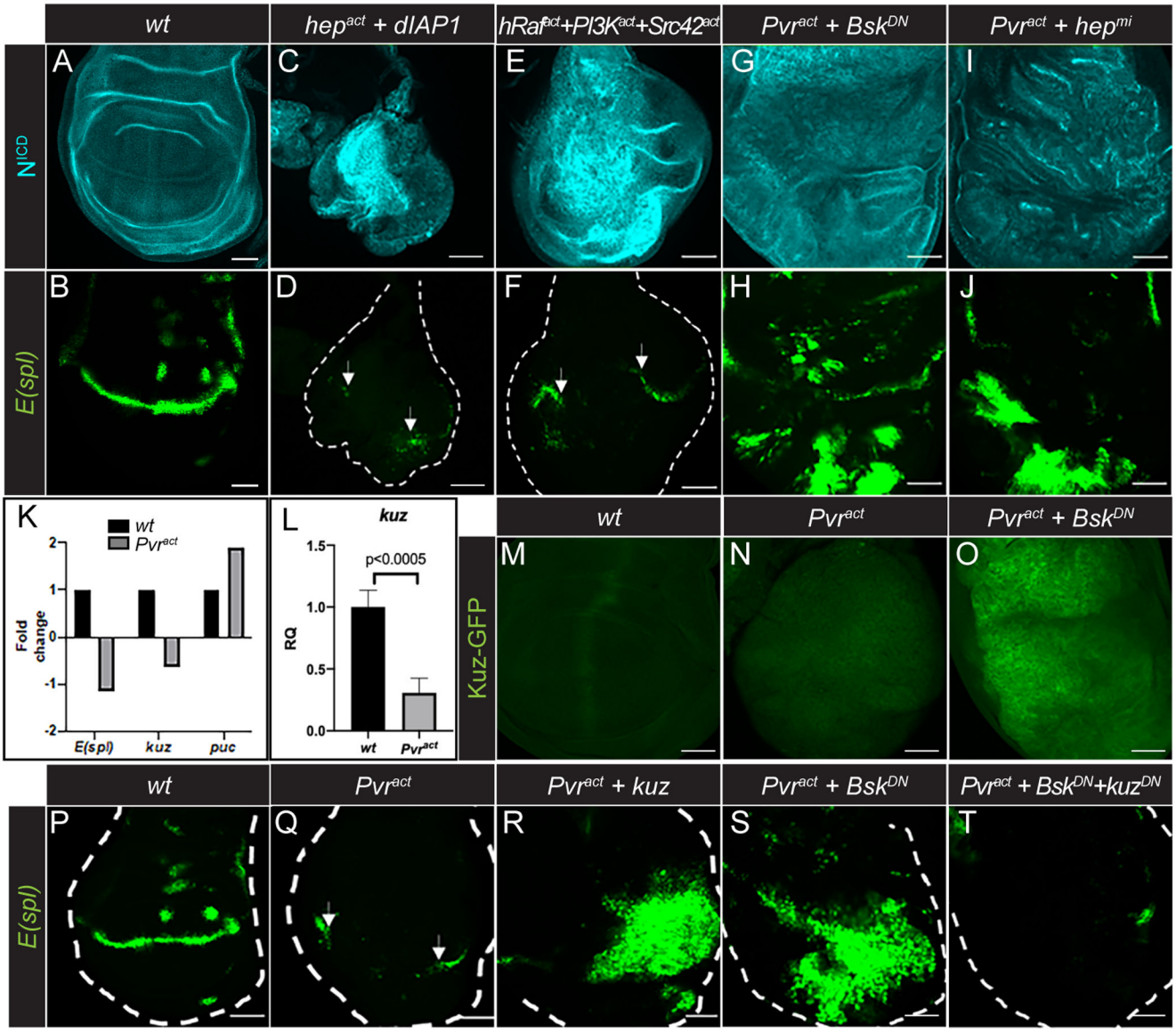

Fig. 3. JNK, but not PI3K or Raf, controls Notch activity through negative regulation of Kuzbanian

(A-J) N^{ICD} (cyan; **A,C,E,G,I**) and *E(spl)m8-GFP* reporter (green; **B,D,F,H,J**) expression in wild-type wing discs (**A-B**), wing discs with constitutive JNK activation (*dpp-GAL4>UAS-hep^{act},UAS-dIAP1*; **C-D**), constitutive ERK, PI3K and JNK activation (*dpp-GAL4>UAS-hRaf^{act},UAS-PI3K^{act},UAS-Src42^{act}*; **E-F**), and combined Pvr activation and inhibition of JNK (*dpp-GAL4>UAS-Pvr^{act},UAS-Bsk^{DN}*; **G-H**, and *dpp-GAL4>UAS-Pvr^{act},UAS-hep^{mi}*; **I-J**) along the A/P axis. Arrows in **D** and **F** point to *E(spl)m8-GFP* expression outside of the *dpp*-expressing region. Note that *E(Spl)GFP* appears distorted and patchy due to extensive growth of the pouch in B, H and J.

(K) *E(spl)*, *kuz* and *puc* transcript levels from RNA-Seq analysis of wild-type (black bars) and *Pvr^{act}* (grey bars) wing discs.

(L) Quantitative real-time PCR analysis of *kuz* levels in wild-type (black bar) and Pvr^{act} (grey bar) wing discs. Data represents mean ± SD (N=3).
(M-O) Kuz-GFP expression in *wt* (**M**), Pvr^{act} (**N**) and $Pvr^{act}+Bsk^{DN}$ (**O**) wing discs.
(P-T) *E(spl)m8-GFP* reporter expression in *wt* (**P**) and Pvr^{act} (**Q**) wing discs, wing discs with combined Pvr activation and overexpression of *kuz* (*dpp-GAL4>UAS-*Pvr^{act}*,UAS-kuz;* **R**), $Pvr^{act}+Bsk^{DN}$ (**S**) and Pvr activation combined with JNK and Kuz inhibition (*dpp-GAL4>UAS-*Pvr^{act}*,UAS-*Bsk^{DN}*,UAS-*kuz^{DN}; **T**). Arrows in **Q** point to *E(spl)m8-GFP* expression outside of the *dpp*-expressing region.
Each staining was repeated 3 times (N=3) and between 5 and 15 samples were analyzed per repeat. Scale bars: 50μm.

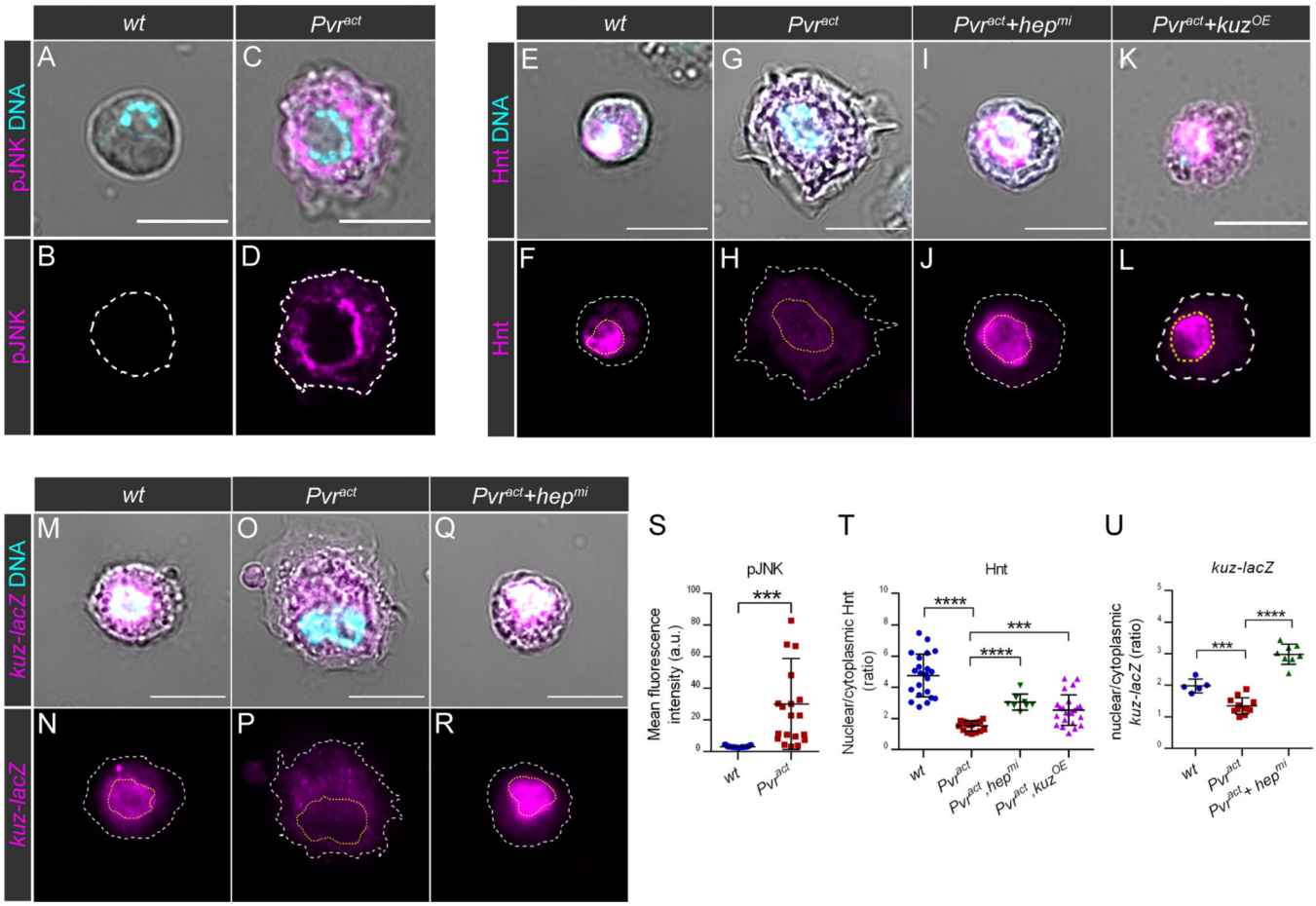

Fig. 4. JNK inhibits Notch activity in *Drosophila* blood cells through negative control of Kuzbanian expression

(A-R) Immunostaining of *Drosophila* circulating larval crystal cells (CCs) in which transgenes are expressed under the control of the *lz-GAL4* driver. In all images, DNA (cyan) was labeled with DAPI and was used to outline the nucleus contours (yellow dashed lines). DIC images were used to outline the cell contours (white dashed lines). Scale bars: 10μm.

(A-D) Activity of the JNK pathway assessed by immunostaining of pJNK (magenta) in CCs of the following genotypes: *lz-GAL4>UAS-GFP* (*wt*; **A-B**) and *lz-GAL4>UAS-GFP,UAS-pvr^{act}* (*Pvr^{act}*; **C-D**). Images show representative examples from N=6 biological replicates per genotype.

(**E-L**) Immunostaining of Hnt (magenta) in CCs of the following genotypes: *lz-GAL4>UAS-GFP* (*wt*; **E-F**), *lz-GAL4>UAS-GFP,UAS-pvr^{act},UAS-mCherry^{RNAi}* (*Pvr^{act}*; **G-H**), *lz-GAL4>UAS-GFP,UAS-pvr^{act},UAS-hep^{mi}* (*Pvr^{act}+hep^{mi}*; **I-J**) and *lz-GAL4>UAS-GFP,UAS-pvr^{act},UAS-kuz* (*Pvr^{act}+kuz^{OE}*; **K-L**). Images show representative examples from N=6 biological replicates per genotype.

(**M-R**) Immunostaining of β-galactosidase, as a readout for *kuz-lacZ* expression (magenta) in CCs of the following genotypes: *lz-GAL4>UAS-GFP,kuz-lacZ* (*wt*; **M-N**), *lz-GAL4>UAS-GFP,UAS-pvr^{act},kuz-lacZ* (*Pvr^{act}*; **O,P**) and *lz-GAL4>UAS-GFP,UAS-pvr^{act},UAS-hep^{mi},kuz-lacZ* (*Pvr^{act}+hep^{mi}*; **Q-R**). Images show representative examples from N=4 biological replicates per genotype.

(**S**-**U**) Quantitative analysis of data represented in (**A**-**R**). Data points in scatter plots correspond to individual cells and lines indicate the mean and standard deviation. Unpaired t-tests were used to evaluate statistical significance, denoted as *** for $p \leq 0.001$ and **** for $p \leq 0.0001$.

(**S**) Quantification of the mean fluorescence intensity associated with pJNK immunostaining in *wt* CCs and Pvr^{act} CCs.

(**T**) Quantification of nuclear Hnt, shown as the ratio of the mean fluorescence intensity associated with Hnt in the nucleus over the mean fluorescence intensity associated with Hnt in the cytoplasm in *wt*, Pvr^{act} (N=16), $Pvr^{act}+hep^{mi}$ and $Pvr^{act}+kuz^{OE}$ CCs.

(**U**) Quantification of nuclear *kuz-lacZ* expression, shown as the ratio of the mean fluorescence intensity associated with β-galactosidase in the nucleus over the mean fluorescence intensity associated with β-galactosidase in the cytoplasm in *wt*, Pvr^{act} and $Pvr^{act}+hep^{mi}$ CCs.

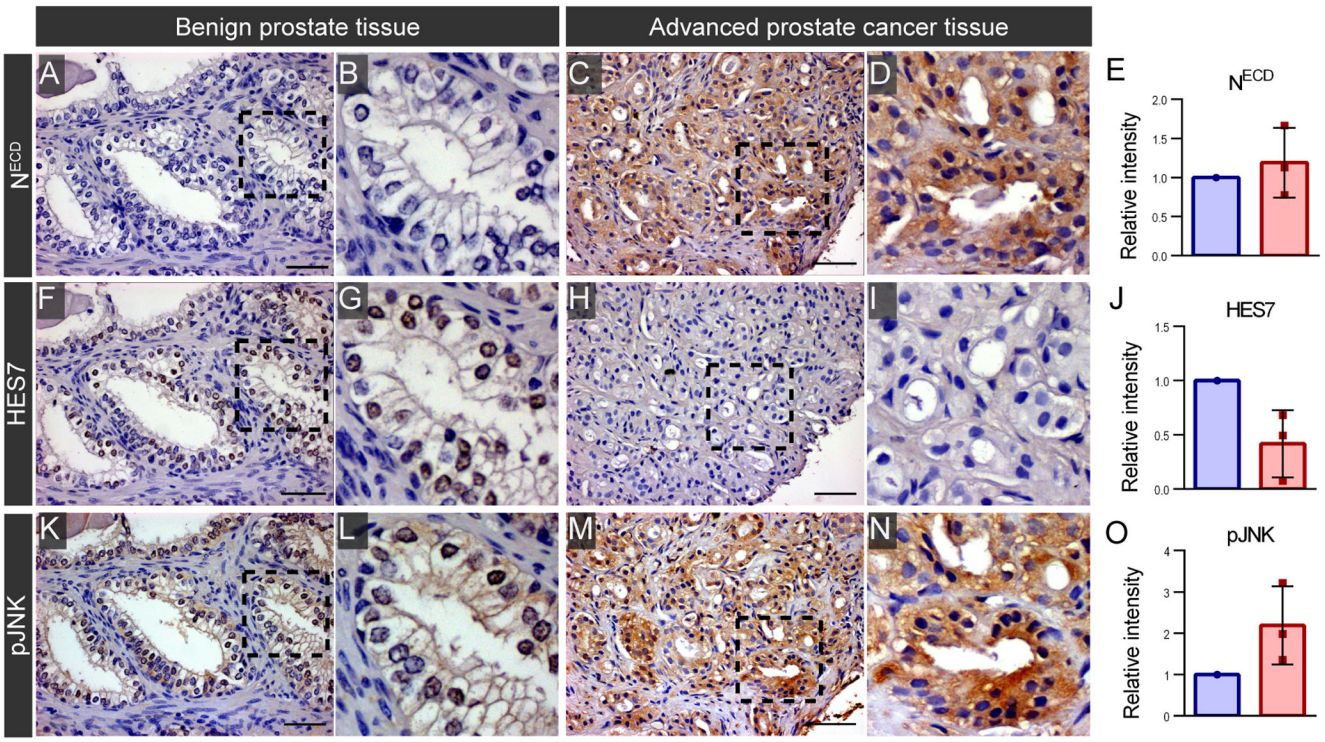

Fig. 5. Low Notch activity correlates with high JNK activity in human prostate cancer tissues.

(**A-E**) Immunohistochemical staining of Notch 1 with an antibody directed against the extracellular domain (N^{ECD}; brown staining) in paraffin sections of benign (**A-B**) and advanced prostate cancer (**C-D**) tissues, with quantification of the mean relative intensity associated with the staining (**E**), represented as the fold change between the average signal in benign prostate tissue (N=3, blue) and advanced prostate tumors (N=3, red).

(**F-J**) Immunohistochemical staining of HES7 (brown staining) in paraffin sections of benign (**F-G**) and advanced prostate cancer (**H-I**) tissue, with quantification of the mean relative intensity associated with the staining (**J**), represented as the fold change between the average signal in benign prostate tissue (N=3, blue) and advanced prostate tumors (N=3, red).

(**K-O**) Immunohistochemical staining of phosphorylated JNK (pJNK; brown staining) in paraffin sections of benign (**K-L**) and advanced prostate cancer (**M-N**) tissue, with quantification of the mean relative intensity associated with the staining (**O**), represented as the fold change between the average signal in benign prostate tissue (N=3, blue) and advanced prostate tumors (N=3, red).

Images in B, D, G, I, L and N are higher magnification of the regions framed with dashed lines in the corresponding A, C, F, H, K and M images. Scale bars: 100μm. Hematoxylin staining, enriched in nuclei, is in purple/blue.

Bar graphs in E, J and O represent the mean value and the standard deviation, based on a benign sample (blue) compared with three independent advanced tumor samples (red).

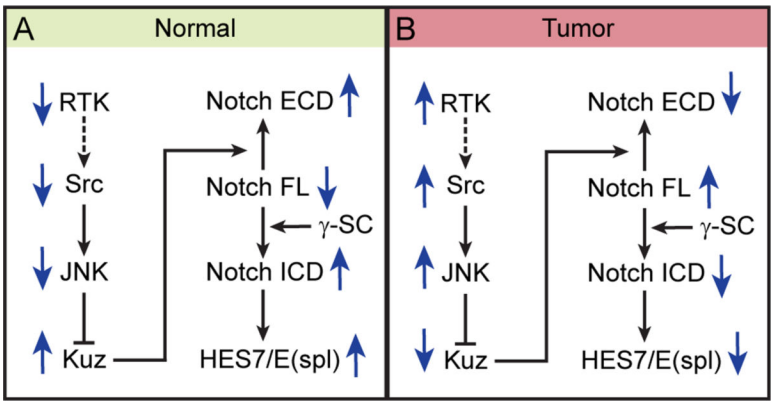

Fig. 6. Model for control of Notch function by activated JNK in tumors

Proposed model based on the observations made in *Drosophila* tumors, in human prostate cell lines and in patient-derived tissue samples:

(A) In normal/benign tissue in which the Notch pathway is homeostatically active, sequential proteolytic cleavages of the Notch receptor activate downstream target proteins that are important for controlled development. The stress-responsive JNK pathway is usually inactive.

(B) In advanced tumors, activating mutations in Src/JNK (or that of a kinase that activates Src/JNK) inhibit proteolytic cleavages of the Notch receptor, by negatively regulating the expression of the S2 cleavage protease (Kuzbanian in *Drosophila*), resulting in a loss of Notch target effector function and an accumulation of the full-length receptor.